The quest for reference stations at the National Observatory of Athens, Greece

Olga-Joan Ktenidou[1], Erion-Vasilis Pikoulis[12], Antonia Papageorgiou[12], Fevronia Gkika[1], Spyros Liakopoulos[1], Ziya Cekinmez[13], Panagiotis Savvaidis[14], Kalliopi Fragouli[15], Fanis Chalaris[1], Christos Evangelidis[1]

[1]Institute of Geodynamics, National Observatory of Athens, Lofos Nymfon-Thiseion, Athens, 11850, Greece
[2]University of Patras, Patras, 26504, Greece
[3]National Technical University of Athens, Athens, 15780, Greece
[4]Aristotle University of Thessaloniki, Thessaloniki, 54124, Greece
[5]University of the Aegean, Mytilene, 22510, Greece

Correspondence to: Olga-Joan Ktenidou (olga.ktenidou@noa.gr)

Abstract. The assumption of reference station conditions is investigated for the first time across 60 rock stations belonging to the broadband and accelerometric networks of the National Observatory of Athens. Provided their data have been publicly available for long enough to yield a substantial number of recordings, we include in our assessment all stations that have some probability of lying on rock, based on existing data or beliefs. No site effects studies have been conducted before for the ensemble of the stations. Furthermore, no ad hoc field campaigns have been performed to characterise them, save in few cases. The first step is to compile all readily available information from publicly available external sources, i.e.,geology, topography, station installation, Vs_{30} estimates and any other known metadata per station. The second step is to analyse external sources, namely geological maps, to derive the geological unit and age, and to combine this information with internal sources, namely questioning the network staff to access the operator's first-hand experience of the sites, to better describe geology, geomorphology, and station installation details. The third and largest step is to compile the first Greek ground-motion dataset on rock and to perform a detailed analysis of the recordings to estimate site-specific amplification to assess local site response characteristics for each station. A strong-motion dataset of over 7500 recordings is developed and curated for this purpose, dating from 2012 to 2023. It is visually inspected and meticulously processed on a waveform-specific basis in the time and frequency domains, paying special attention to signal quality and the relation to noise. Single-station amplification functions (horizontal-to-vertical spectral ratios, HVSR) are estimated from the database, and the site resonance characteristics are assessed. Considering that 'true' reference site behaviour implies low, flat amplification with no directional dependence, the analysis goes beyond the usual path of combining the two horizontal components into a mean HVSR: it also assesses the directional sensitivity of the HVSR to identify departure from the 1D assumption, it corrects the HVSR for the vertical amplification effect, and uses clustering techniques to select groups of stations with different response characteristics. These data-derived characteristics are combined with the previously compiled station metadata, and they all constitute criteria that are co-assessed to evaluate the stations' overall capacity as reference sites. This results in a qualitative

ranking of the stations. The least and most desirable reference stations are showcased, hoping to facilitate a better use of seismic data in future seismological and hazard applications.

1 Introduction

1.1 The need for station characterisation and reference stations

The importance of understanding site conditions at strong-motion recording stations, which often lie on soft soils, has been known for decades. Important global databases such as NGA-West2 (Ancheta et al., 2014) made a point of procuring rich and homogeneous station metadata in terms of Vs, depth to bedrock, etc. Ground motion models have moved towards more detailed descriptors of station conditions, and a global effort is being made in characterising strong-motion stations. On the contrary, seismological stations are typically installed on rock sites and assumed free of any site effect. Hence there is rarely any effort to characterise them or challenge their quality as reference stations. Recently, strong-motion and broadband seismological data have been used together more and more often, as the limits between the different sensor capabilities are beginning to blur and the magnitudes of interest are beginning to drop. Hence, it is a good time to ask the question of whether the scrutiny traditionally applied to strong-motion station conditions may begin to apply also to seismological stations.

In recent years, particular importance has been attached to assessing ground motion on rock sites in particular, while in the past it was considered as rather homogeneous (some notable exceptions including the seminal works of Silva & Darragh 1995 and Steidl 1996). We now recognise that material properties and geometry –the main ingredients of site response- can cause ground motions to differ strongly between rock stations, and that they are not as 'uninteresting' as we once thought in terms of site response (i.e., the implicit assumption of negligible amplification dos not hold). This has important potential impact on reference ground motions and the definition of reference stations, which once were simply defined as those coming from 'rock' sites. It has impacted seismic hazard and risk assessment for significant structures and critical infrastructures, which now often accounts in detail for such rock property variations. However, rock sites can be notoriously challenging to characterise, and many networks have not characterised their rock stations, as priority had been initially –and reasonably- given to stations lying on soils.

Some studies in the past decade or so attempted to focus on rock sites. Van Houtte et al. (2012) tested stations in Christchurch that were typically used as reference stations without previous checks, by computing site transfer functions. Ktenidou & Abrahamson (2016) found broadband amplifications even in CENA rock sites that had been considered as extremely hard (Vs_{30} of 2000 m/s). More recently, much more systematic and large-scale efforts have been made on European level by Lanzano et al. (2020), who made a large-scale detailed effort for defining reference sites in Central Italy using various proxies as well as transfer functions from seismic data and noise, as did Pilz et al. (2020) who also included artificial intelligence tools in their reference site identification. Di Giulio et al. (2021) attempted to assess in a systematic

way the seismic station characterisation efforts across Europe in terms of data quality, methodological reliability etc., emphasising the importance of consistency.

1.2 Motivation of this study

The new European Seismic Hazard and Risk Models, also known as ESHM20 (Danciu et al., 2021) and ESRM20 (Crowley et al., 2021), were published recently. The latter includes an empirical amplification model at a European scale (Weatherill et al., 2023) to account for site effects with respect to rock conditions, which relates to Vs_{30}. In Greece, Pitilakis et al. (2024) recently proposed a new seismic hazard zonation map to potentially be considered in the new national annex that will accompany the version of Eurocode 8 (CEN 2004). These zones were defined with respect to rock conditions so as to be used for seismic actions in different geotechnical/geological contexts. From the EC8 point of view, Labbe and Paolucci (2022) reported that the new site classification drafted included not only amendments to soil classes, but also an additional parameter to defining the rock class, which was the fundamental frequency. The definition of soil conditions is of necessity relevant to the definition of rock, and the latter is acquiring more prominence lately. A large scope of models and applications are affected by such definitions, including ground motion models, seismic hazard maps, shakemaps, etc. So, again, it is a good time to consider the question of reference sites.

Although Greek data are of great importance to European and even global ground-motion datasets, relatively little progress has been made in the digital era in characterising stations. Many logistical reasons lie behind this, including the fact that a significant number of seismic networks are run by different operators exist (Evangeldis et al., 2021), there is a large number of stations off the mainland or in areas that are difficult to approach due to terrain, etc. Some efforts have been made to compile what station metadata exist, since the early days of HEAD, the first strong-motion database (Theodoulidis et al., 2004). Margaris et al. (2014) provided a brief history of the characterisation of Greek strong-motion stations with boreholes, geophysical campaigns and microtremors, while Stewart et al. (2014) compiled values of Vs_{30} and other site descriptors for some strong-motion stations, mostly based on information within a 1-km radius from the stations per se. Margaris et al. (2021) include the most up-to-date version of available strong-motion station metadata, mostly through proxies. We note that the ensemble of stations considered in all the above studies includes a large number of stations that lie on soft ground, and a large fraction of them are not yet publicly available through European waveform services (ESM). Only one systematic effort was made so far, for one of the Greek networks (HI, doi:10.7914/SN/HI; ITSAK, 1981) by Grendas et al. (2018), in which the actual strong-motion recordings were analysed to compute empirical transfer functions to understand site amplification; however, the majority of those stations are again not publicly available in terms of waveform data.

The goal of this work is to focus on the networks of the National Observatory of Athens (doi:10.7914/SN/HL; NOA-GI, 1975), including not only the strong-motion one (https://accelnet.gein.noa.gr) but also the broadband seismic one (https://bbnet.gein.noa.gr/HL/), and further focus on the stations openly available in real-time continuous mode through the EIDA@NOA node (Evangelidis et al., 2021). For a fraction of the strong-motion stations, site conditions are known in great detail thanks to geophysical in situ investigations conducted in the recent national project HELPOS (Hellenic Plate

Observing System); however, most of these stations are either not open or lie on soils. To date, most of the openly available strong-motion stations are still characterized via proxies, while none of them have been analysed to determine empirical amplification functions (spectral ratios). Moreover, there has never been a systematic, consistent effort to include broadband stations as well, despite the increasing importance that is recently being attached to broadband data in ground-motion databases. In the HL networks, only a few small-scale efforts were made in the recent past to understand the behaviour of selected strong-motion and broadband stations using the recordings themselves (Ktenidou & Kalogeras, 2019; Ktenidou et al., 2021a, 2021b). These were made using only limited datasets, mostly as proof of concept to the work at hand. This paper marks the beginning of a more systematic study of the NOA network conditions, starting with rock sites.

2 Strong-motion data and analysis

2.1 Station and data selection

All stand-alone broadband stations (HH channels) and all collocated broadband and strong-motion stations (HH and HN channels) are generally thought to lie on rock conditions. Hence all such stations are included in this study, as long as they had enough recordings at the end of 2023, which could be publicly accessible via the EIDA@NOA node at that time (Evangelidis et al., 2021). In addition, we considered all stand-alone strong-motion stations (HN) open to the public via EIDA, and selected all those for which some indication could be found of them lying on rock. Such indications included literature and online resources, geological map information, proxy-based information, operator's information, site visit information, etc. The rationale behind this generous and inclusive selection process was simple: we would rather include more stations than are actually reference sites and dismiss them later after detailed scrutiny, than miss out on any potential reference stations due to strict initial criteria. The layout of the stations selected is shown in Fig. 1, and some basic information about them is compiled in Table 1 (where 'HNc' indicates strong-motions stations installed at the same site as a broadband station).

Table 1. General information and metadata for the stations in this study and statistics on the ground-motion data analysed.

Station Name	Network code	StLat (deg)	StLon (deg)	StEl (m)	Period	ML range	Repi range (km)	Azim. gap (deg)	Nrec
AMORGOS	HL	36.83156	25.89384	308	2012-2019	4.0-6.2	24-403	27	59
ANTIKYTHIRA	HL	35.86704	23.30117	143	2012-2023	4.0-6.6	23-492	48	117
APEIRANTHOS, NAXOS	HL/GE	37.07274	25.52301	608	2012-2023	4.0-6.3	21-423	27	183
ARCHANGELOS, RHODES	HL	36.21356	28.12122	148	2012-2023	4.0-6.7	10-366	37	144
ASTYPALAIA	HL	36.54552	26.35295	64	2012-2020	4.0-6.7	9-402	37	107
ATHENS-NEO PSYCHIKO	HL	38.00080	23.77349	187	2020-2023	4.0-6.0	26-345	41	47
DIONYSOS ATTIKIS	HL	38.07794	23.93306	460	2013-2016	4.0-6.3	13-351	52	33

DELFOI	HL	38.47836	22.49583	570	2012-2023	4.0-6.6	7-425	32	341
EVRITANIA	HT	38.91657	21.81050	1037	2012-2023	4.0-6.1	20-392	27	317
GAVDOS	HL	34.83914	24.08738	170	2012-2017	4.0-6.2	3-319	46	86
HERAKLEIO	HL	35.30580	25.07090	45	2017-2021	4.0-6.3	18-214	47	72
ANOGEIA	HL/MN	35.28878	24.89043	750	2012-2023	4.0-5.5	12-352	21	196
AGIOS KIRIKOS IKARIA	HL	37.61117	26.29283	30	2012-2017	4.0-6.3	42-380	50	77
CHANIA, CRETE	HL/GE	35.46060	23.98110	230	2012-2023	4.0-6.2	23-291	27	167
ITHOMI MESSINIA	HL	37.17872	21.92522	423	2018-2017	4.0-6.0	11-420	34	227
IOANNINA	HL	39.65616	20.84874	526	2012-2023	4.0-6.6	12-395	24	182
KARPATHOS	HL	35.54710	27.16106	524	2012-2022	4.0-6.7	4-300	22	290
KASSIOPI	HL	39.74628	19.93542	65	2012-2018	4.0-6.0	27-374	145	73
KERKYRA	HL/MN	39.71270	19.79623	227	2012-2022	4.0-6.6	46-377	167	98
KALYMNOS	HL	36.95708	26.97274	28	2013-2023	4.0-6.7	16-406	48	257
KALAVRITA	HL	38.04350	22.15040	758	2012-2023	4.0-6.6	12-381	21	346
KASTELLORIZO	HL	36.15031	29.58561	64	2012-2021	4.0-6.7	67-458	221	77
KASTELLI, CRETE	HL	35.18010	25.33720	395	2021-2023	3.5-5.7	3-224	61	34
KYTHIRA	HL	36.25660	23.06210	360	2013-2023	4.0-6.2	23-443	39	76
KAVALA	HL	40.93704	24.38591	122	2012-2023	4.0-6.1	73-338	158	58
KYMI	HL	38.63315	24.10014	259	2014-2021	4.0-6.7	36-519	25	99
KOZANI	HL	40.30331	21.78209	791	2012-2023	4.0-5.9	53-384	73	134
LIMNOS	HL	39.89725	25.18055	67	2012-2023	4.0-6.7	19-380	41	113
ATALANTI LOKRIDA	HL	38.64957	22.99881	192	2012-2023	4.0-6.3	17-349	25	121
MEGANISSI LEUKADA	HL	38.65606	20.79116	58	2012-2014	4.0-5.8	17-232	115	75
PLAKA, MILOS ISLAND	HL	36.68984	24.40171	175	2012-2023	4.0-6.3	33-407	29	201
NEOCHORI VOLOS	HL/MN	39.30567	23.22189	510	2012-2023	4.0-6.3	35-358	19	152
NISYROS ISLAND	HL	36.61060	27.13090	44	2021-2021	4.0-6.7	11-282	79	114
VOLCANOGOLY MUSEUM, NISYROS	HL	36.57441	27.17666	423	2021-2022	4.1-5.7	73-282	189	**11**
ATHENS- THISSEIO	HL	37.97384	23.71767	93	2012-2018	4.0-6.3	18-399	27	151
NEAPOLIS CRETE	HL	35.26134	25.61037	288	2012-2023	4.0-6.2	27-398	37	97
KATO NEVROKOPI	HL	41.34846	23.86517	627	2012-2023	4.0-6.3	43-449	83	52
ORTHONIES, ZAKYNTHOS	HL	37.85112	20.69627	450	2018-2023	4.0-5.9	22-310	47	65
PENTALOFOS KOZANIS	HL	40.19588	21.13842	1096	2012-2021	4.0-6.0	26-261	47	55
POLIGIROS CHALKIDIKI	HL	40.37328	23.44443	566	2013-2013	4.0-6.3	20-361	96	58
AGIA PARASKEVI LESVOS	HL	39.24565	26.26499	130	2013-2023	4.0-6.7	11-442	44	101
PSARA	HL	38.53978	25.56202	13	2012-2018	4.0-6.3	6-393	39	71
PENTELI	HL	38.04730	23.86380	500	2012-2021	4.0-6.6	29-457	43	142
RODOPI	HL	41.14503	25.53553	116	2012-2020	4.0-6.1	89-364	125	58
RIOLOS KATO ACHAEA	HL	38.05586	21.46475	97	2012-2023	4.0-6.6	10-424	17	354
SIVAS CRETE	HL/GE	35.01777	24.81204	96	2012-2023	4.0-6.3	36-347	40	78
SKYROS	HL	38.88310	24.54820	268	2012-2022	4.0-6.3	28-370	39	70
SAMOS	HL	37.70425	26.83772	348	2020-2023	4.0-6.3	14-357	93	58

SAMOTHRAKI	HL	40.47094	25.53045	365	2012-2023	4.0-6.7	20-313	123	71
TETRAKOMO	HL	39.34450	21.27467	942	2018-2023	4.0-5.9	56-345	33	72
ANCIENT THERA, SANTORINI	HL/GE	36.36699	25.47526	288	2019-2023	4.0-6.3	34-481	39	104
KLOKOTOS	HL/MN	39.56468	22.01440	86	2012-2023	4.0-5.4	58-202	32	119
IEK THIVAS	HL	38.32983	23.33601	214	2020-2023	4.0-5.9	49-392	68	45
TINOS	HL	37.53942	25.16310	21	2012-2023	4.0-6.7	76-393	36	152
VAMOS	HL	35.40700	24.19970	225	2012-2023	4.0-6.3	32-277	35	170
VELIES LAKONIA	HL	36.71803	22.94686	220	2012-2023	4.0-6.2	11-399	19	150
VOLIMES- ZAKYNTHOS	HL	37.87670	20.66293	431	2014-2015	4.0-5.8	34-139	83	56
VALSAMATA KEFALONIA	HL	38.17683	20.58860	402	2012-2023	4.0-5.9	20-387	33	220
BOYLA ATTIKHS	HL	37.85240	23.79420	256	2012-2022	4.0-6.3	32-411	38	103
ZAKROS	HL/GE	35.11470	26.21691	254	2012-2019	4.0-6.2	10-470	59	105

A threshold minimum magnitude of ML4 was considered for each station, dropping down to M3.5 only in one case, for a station installed in 2021. The maximum distances considered varied according to noise level and station population of recordings, but scaled from out to 150 km for smaller events and out to 300 km or more for large events. The overall M-R distribution is shown in Fig. 2a for the ensemble dataset, with colour darkness indicating density of recordings. Figure A1 of the Supplement shows the M-R distribution for all stations in alphabetical order, starting with AMGA.HN and so forth. Because the purpose of this dataset is the study of site effects (not, for instance, the development of ground motion models) and the M-R distributions are used as an indication only, we use local magnitude scale and epicentral distance metrics and do not go into the details of moment magnitude and rupture distance for the large events in the dataset. A total of 7512 three-component recordings are analysed in this study, coming from 1364 earthquakes. The number of records per station is shown in Fig. 2b. The minimum number of usable recordings for the single least populated station is 11, the mean number of recordings is 125, while some stations have more than 300.

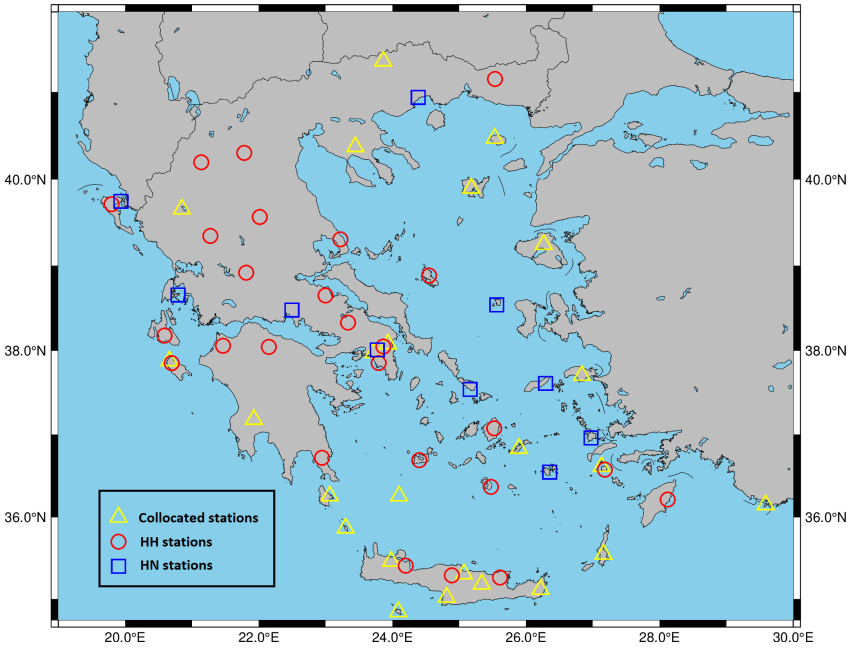

Figure 1: Map of selected HL stations (believed to lie on rock, with publicly available data via EIDA@NOA and adequate number of events).

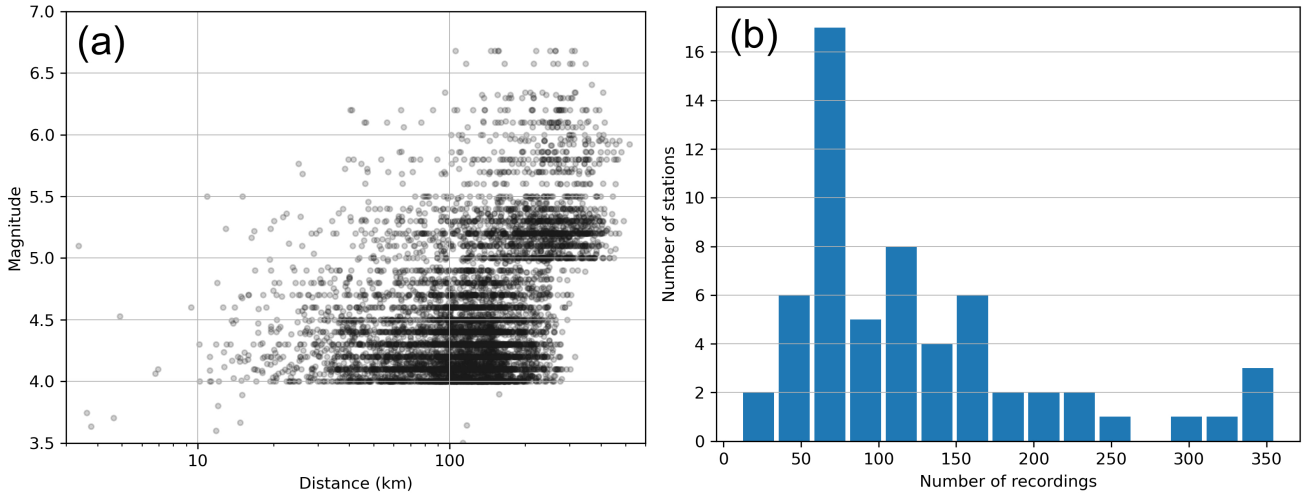

Figure 2: a. Indicative distribution of magnitude (local) and distance (epicentral) for all data analysed in this study. Station-specific plots can be found in the Supplement (Figure A1). b. Histogram of the number of recordings used per station.

2.2 Data processing and creation of a new strong-motion dataset

The data we select come from the period 2012-2023, depending on when each station began to operate in real-time, its period of operation and data availability. We use the catalogue of NOA (https://eida.gein.noa.gr/fdsnws/availability/1) and search for recordings following the criteria mentioned above. We retrieve raw waveforms and station xml from

EIDA@NOA and apply instrument correction to retrieve physical units. We then develop a workflow for the data processing that is inspired by the rationale described in Kishida et al. (2016), the procedure that underpins the NGA-East processing (Goulet et al., 2014). The developed procedure differs significantly from the manual processing protocols elsewhere, such as the European services (ESM; Lanzano et al., 2021; Luzi et al., 2016), because here comparison of signal quality with respect to noise at both high and low frequencies is paramount. We develop our own in-house software to fit the purpose for analysis in the time and frequency domain and the main steps we follow are described below:

1. We first check raw broadband (HH) data for clipping and discard all such instances. This is not relevant for strong-motion (HN) data.
2. We then perform visual inspection on all instrument-corrected waveforms in the time domain to discard obvious problematic cases (low quality, component errors, et.c). We note that we treat instances of 'double events' (two earthquakes occurring one right after another, leading to interference of the various wave packages) on a case-to-case basis, salvaging cases where possible.
3. We perform windowing: Expected theoretical P and S arrival times are first automatically computed based on the origin time and location of each event. Coda window onset is also computed although not used in this work. S-wave duration is estimated based on magnitude and distance, and a similar duration is chosen for the pre-event noise window.
4. Theoretical window markers are automatically plotted on the seismogram as dotted lines (Figure 3 - top), and the analyst assesses and amends them as needed (solid lines). Note that we aim for the signal window to include all wave packages of engineering interest, i.e. all S waves and the most energetic surface waves. Appropriate allowances are made for the tapering not to affect S arrivals.
5. We then cut the pre-event and signal windows and taper them, before computing Fourier amplitude spectra (FAS) of acceleration for both. We smooth them using the Konno & Ohmachi (1998) technique with a mild b=40. We compute the signal-to-noise ratio (SNR) on the smoothed FAS for each component. We note, however, that in the low frequencies the SNR is not necessarily the best indicator because of the small number of points, hence we rely heavily on visual inspection of the FAS.
6. We perform visual inspection in the frequency domain, assessing both the smoothed and unsmoothed acceleration FAS of the signal, the noise, and 3 times the noise spectra, in log and linear scale respectively (Figure 3 – middle and bottom). Aside from the signal-to-noise ratio (SNR=3 threshold), we also consider the fit to the omega-square source model (Brune 1970; 1971) in the low-frequency band.
7. We select the lowest and highest usable frequencies (LUF, HUF). If one were to use time series, these are the filter corners that one would use for the filtering. As it stands in this work, we work in the FAS domain so we need not filter. But we take great care that all FAS we use to compute empirical transfer functions in the next step are used strictly within their usable frequency per waveform. This way, for each frequency, the results are reliable and we can guarantee that they carry no noise-related artefacts.

This leads to the creation of a new database of over 7500 three-component recordings that includes the hand-picked usable bandwidths of all recordings of events >M4 for the 60 potential reference stations of the HL network that were available until the end of 2023. Because the focus in creating it was the meticulous study of the corner picks, this database can be used with confidence by those seeking to exhaust the usability of recordings at the low and/or high end of the spectrum.

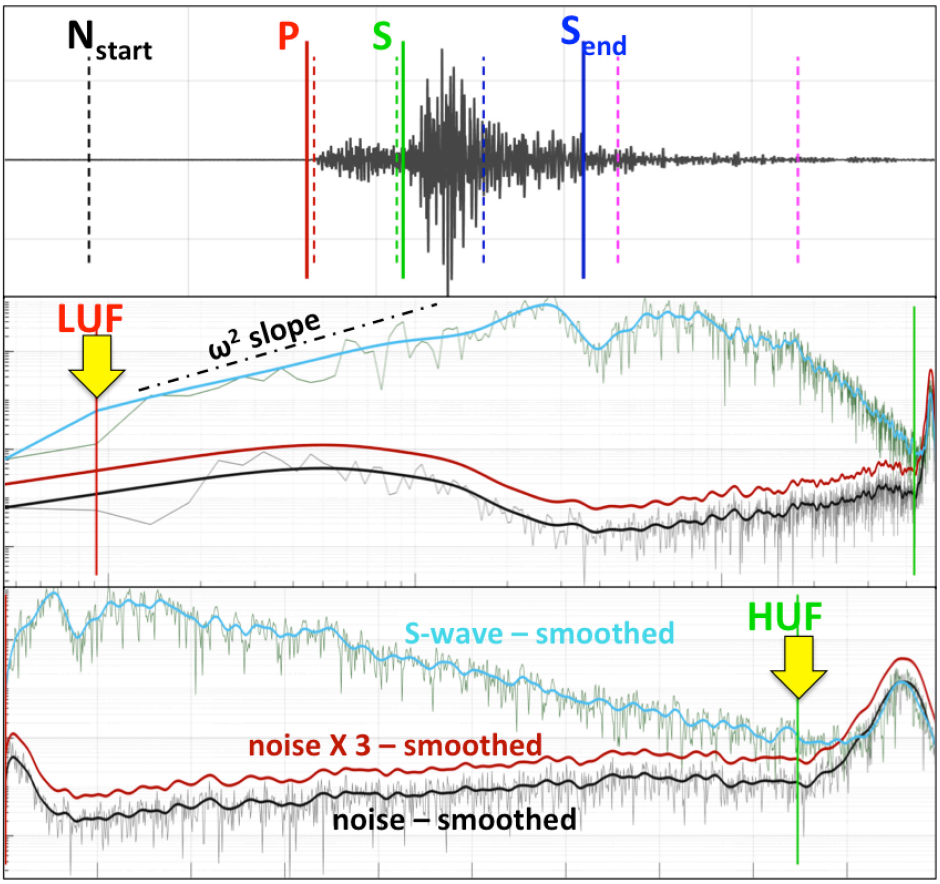

Figure 3: Example of manual processing. Top: windowing of a velocity trace in the time domain, selecting the beginning of the noise and S windows and the end of the S window. Middle and bottom: selecting the lowest usable and highest frequencies (LUF and HUF) in the frequency domain in log and linear scale respectively on the acceleration FAS.

3 Empirical transfer functions

3.1 Orientation-independent HVSR

We compute the horizontal-to-vertical spectral ratio (HVSR; Lermo & Chavez-Garcia, 1993) for each component of each recording at each station. We compute the spectral ratios of the horizontals with respect to the vertical in the same manner as

the SNR: the start of the S-wave windows is taken early enough so as for the first S waves not to be affected by the tapering, and the acceleration FAS are computed and smoothed with a Konno & Ohmachi (1998) b=40 mild smoothing. The mean HVSR per site is computed as the logarithmic average across all events, as is customary, and given that Ktenidou et al. (2011) showed that empirical spectral ratio ordinates are lognormally distributed. At each frequency, the mean is computed strictly out of the recordings available within the legitimate bandwidth, which means that the contributing number of earthquakes varies with frequency. Within the range of 1-10 Hz, typically all recordings are usable, while as noise increases towards lower and higher frequencies, fewer recordings are strong enough to contribute. The FAS of the two horizontal components are combined for each recording as the square root of the sum of squares (SRSS) so as to yield an orientation-independent estimate that does not depend on how the sensor was installed. Fig. 4 (top) shows two examples of this rotation-invariant mean HVSR ±1 SD. We draw the inset on top to indicate the number and percentage of usable recordings per frequency: e.g., for APE station, a total of 183 earthquakes contribute to the HVSR in the range of 0.9-9 Hz, and less than 25% of that (46 earthquakes) at frequencies below 0.07 Hz and above 25 Hz. We note that the curves and their ±1 SD uncertainty (shaded area around the mean) are only drawn for frequencies where the number of usable events is at least 5, in order to ensure a more robust estimate of the statistics (most ground motion applications will accept a minimum of 3). Figure A2 in the Supplement shows the rotation-invariant mean HVSR results for all of our 60 stations in alphabetical order.

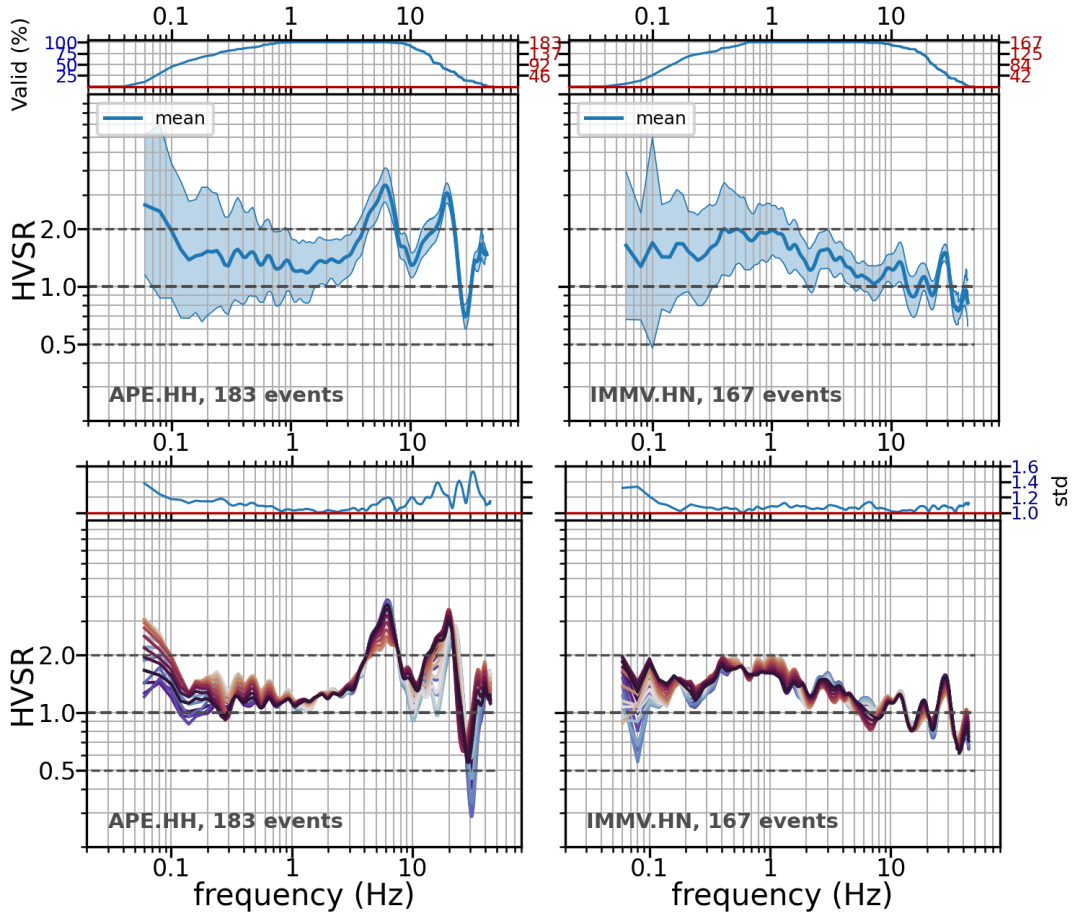

Figure 4: Example HVSR results for stations APE.HH (left) and IMMV.HN (right). Top row: mean, orientation-independent (SRSS) HVSR ±1 standard deviation; the inset on top indicates the number and percentage of usable recordings per frequency. Bottom row: HVSR per component, as those are rotated by 10-degree intervals from North to East; inset on top indicates the standard deviation (hence, directional sensitivity or variability) per frequency.

Let us now study the shape of the HVSR results in Figure 4 (top). A reference site is expected to exhibit a HVSR that is relatively flat and close to unity. Departure from reference site conditions has been judged in different ways across different studies. A few example thresholds include the typical value of HVSR>2, but also HVSR>2√2=2.8 (Lanzano et al., 2020 from Puglia et al., 2011), and the slightly more generous one of HVSR>3 (Pilz et al., 2020). Of course, HVSR is an approximation, and generally an underestimation with respect to the 'true' site transfer function, for instance as that may be computed using the standard spectral ratio (SSR) of Borcherdt (1970), i.e., using an actual rock recording as reference rather than the vertical. The assumed premise of HVSR is not necessarily that the vertical component actually remains completely unaltered by stratigraphy (or, indeed, by other geomorphological features), but rather that it is expected to exhibit amplification at frequencies higher than the ones the horizontal ground motion amplifies around (typically at √3 times the

resonant frequency of the horizontal S waves). Thus it permits a rather clear identification of at last the first resonant peak of the S waves, albeit at a generally lower level than the actual.

In our case, the value of $2\sqrt{2}$ is mathematically more appropriate, given the fact that we computed SRSS of the two horizontal N and E components, corresponding to the hypotenuse of the two orthogonals. So in studying our mean HVSR results across our stations, we could use a threshold of HVSR>$2\sqrt{2}$ when attempting to identify significant resonant peaks and a stricter threshold of (relatively flat) HVSR<2 in selecting potentially passable reference sites. Based on this rationale, the left-hand case (station APE) in Figure 4 exhibits a clear resonance at 6 Hz with amplitude significantly higher than 2.8, followed by what could even be considered a first higher mode at roughly 3 times that frequency, 20 Hz. This resonance is far from the desired behaviour of a reference site. On the other hand, for the right-hand side case, station IMMV, HVSR is rather flat and less than 2, indicating a passable behaviour. Results such as those shown in the top line of Figure 4 are shown in the Supplement for all of our 60 stations (Figure A2). After studying these results across all stations, in Figure 5 we present the most passable HVSR shapes, flat over a wide frequency range and <2, and conversely, in Figure 6, we present the least passable HVSR shapes, with shapes departing from flat and amplitudes exceeding 2.8 over either a narrow or a broadband amplification peak. Table A1 in the Supplement compiles the resonant frequencies (f_0) and their corresponding amplitude (A_0) that were thus identified, using these criteria. As a comparison, it also shows the f_0 identified automatically by a picker. The table also includes the first resonant peak characteristics (f_1, A_1) for the few cases where they were clearly visible according to the criteria. We do note again that HVSR shape is in itself only a proxy: it is conceivable that an inadequate reference station may have a flat-shaped HVSR, but it is expected that an adequate one will have a flat HVSR.

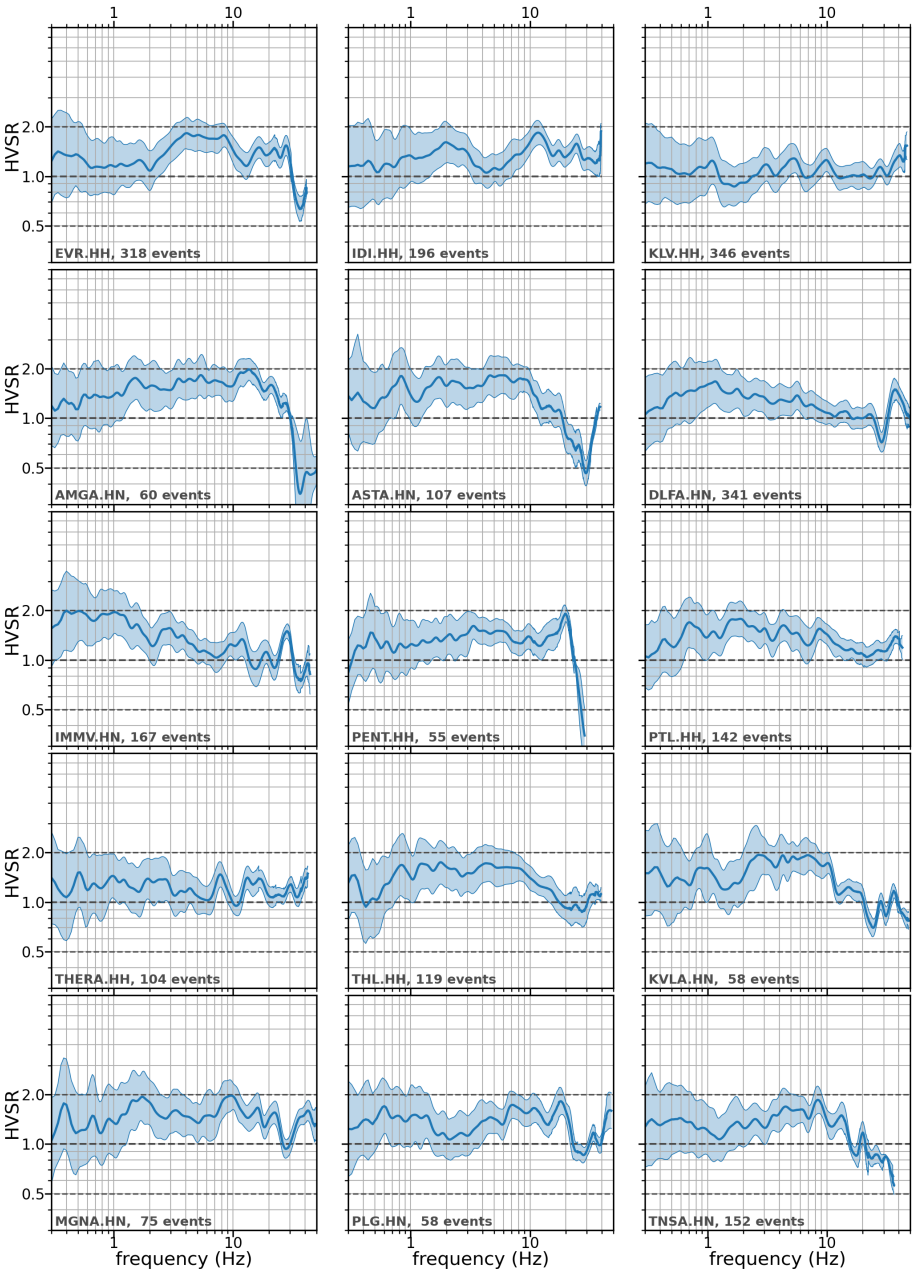

Figure 5: The most passable HVSR shapes, flat over a wide frequency range and amplitudes less than 2.

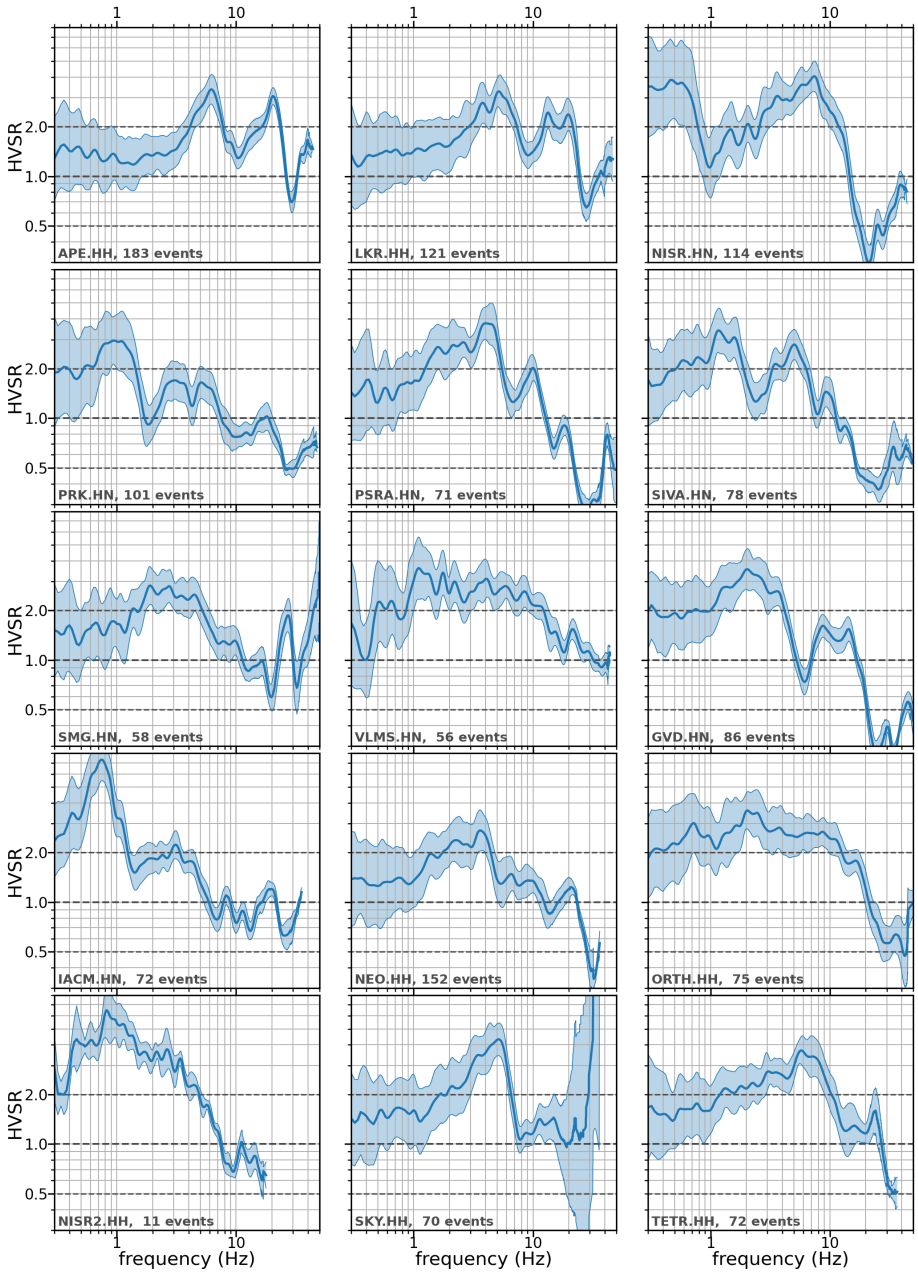

Figure 6: The least passable HVSR shapes, with shapes departing from flat and amplitudes exceeding 3 over either a narrow or a broadband amplification peak.

3.2 Rotational sensitivity of HVSR

We also expect a reference site to not exhibit strong directional dependence, i.e., reference ground motions not to be sensitive to the sensor installation orientation. However, checking only the difference between the two horizontal components as installed is not rigorous enough. The sensors are installed in the N and E directions, which are arbitrary with respect to each site's potential geomorphological features. This is why we follow the technique of Ktenidou et al. (2016) to assess the variability of site response to azimuth. We rotate each time series by successive increments of 10°, from 0°-90°, and recompute the FAS and HVSR each time (yielding a total of 18), so as to discover whether there are any other directions that may bring out directional differences. Such differences we view as an indication of departure from 1D behaviour due to local geomorphology. If there is orientation dependence, it is likely due to and aligned with the direction of the local geomorphological features of the site (basin edges, inclined layering, lateral discontinuities, topography, etc.) and it indicates a departure from 1D behaviour. All of these factors can cause amplification of different levels in the two horizontal components, e.g. the radial and transverse with respect to the feature's axis. Kenidou et al. (2016), e.g., used this successive rotation technique to show that the maximum and minimum amplification level observed near a basin edge occurred in directions parallel and perpendicular to the edge axis.

Figure 7 shows an example of how directionality is quantified in this work. The mean HVSR per component is computed as the as-installed motions are rotated by 10-degree increments from North to East. The inset on top indicates the standard deviation of the man HVSR values across all rotations per frequency. We consider this as an index of the directional variability of each station's site response. Though the typical parameters extracted from such calculations are most of all the resonant frequency f_0, and –to some extent of credibility, mostly as an indication- the corresponding amplitude A_0 and perhaps the same metrics for the first higher mode, if applicable, we also take note of the directional variability of the transfer function amplitude. To this end, we compute the mean of this variability function with frequency across two indicative ranges of interest, namely a wide one spanning two orders of magnitude (0.3-30 Hz) and a narrower one order of magnitude, which may also be more interesting for typical structural response (1-10 Hz). We also note the value of this function around the resonant frequency of the site. We propose that these three values ($SD_{0.3-30}$, SD_{1-10}, SD_{fo}) can be used as approximate indicators of the azimuthal stability of site response. For the site VLS used as an example in Figure 7, these orientation-related scatter in HVSR begins above 10 Hz and thus affects mostly $SD_{0.3-30}$ (1.24) and SD_{fo} (1.48 at 20 Hz). The value of SD_{1-10} (1.12) is relatively low.

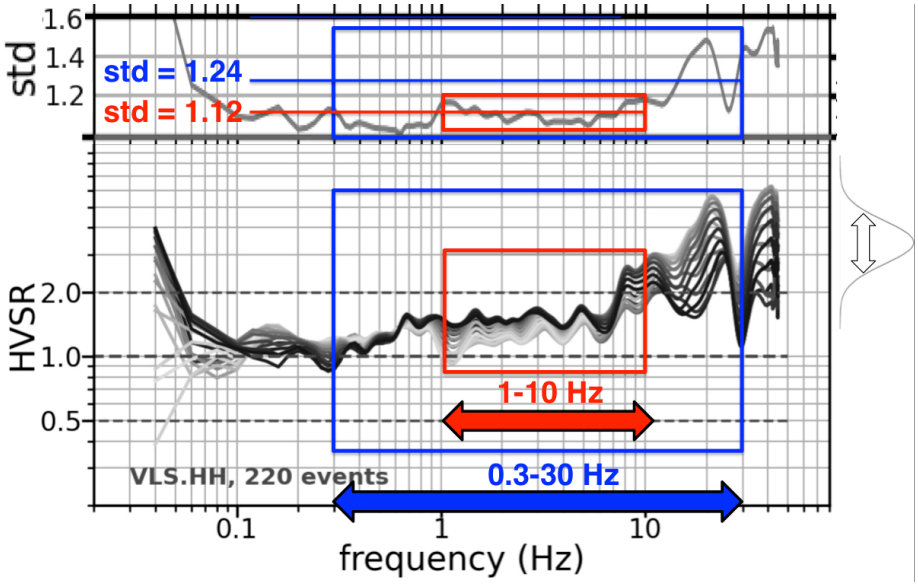

Figure 7: Illustration of the two frequency bands over which the standard deviation from the rotations is averaged, to derive an index of directional variability: 0.3-30 Hz (blue) and 1-10 Hz (red). For station VLS, the value is low for the narrow band (1.12) but high for the wider one (1.24) due to high-frequency variability above 9 Hz.

In the bottom line of Figure 4, we now note the relevant results and can now compare to the orientation-independent mean HVSR from the top line. We now see that station APE, which had already been judged poorly due to its clear strong peaks (amplification peak reaching above 3 based on 183 recordings - top plot), is now seen to also exhibit non-negligible directional variability around its f_0 of 6.1 Hz of around 1.20 (bottom plot). In contrast, station IMMV appears to be a very good candidate for a reference site, lacking not only any identifiable peak (top line) but also and having low directional sensitivity of around 1.07 (bottom line).

Figure 8 illustrates a few characteristic examples of HVSR shape and directional sensitivity. Considered in the band of 0.3-10 Hz, ASTA is the best reference candidate with no amplification and very low SD, followed by VLS, with rather higher variability (yet still a rather acceptable reference below 10 Hz). VLI exhibits a weak but clear low-frequency resonance, while IACM a clear and very strong one, with also a rather clear first higher mode. None of these two show directional variability. KTHA and NISR2, on the other hand, show weak and strong peaks respectively which are rather broadband (not so 'peaky' as their counterparts VLI and IACM), and in addition possess a very high degree of directionality. The behaviour of most of these stations is certainly not what we would expect of 'rock stations'. Based on geological 'labels' indicating rock or the fact of being seismological stations, one might be inclined to consider them a priori as reliable reference stations, assuming they exhibit no amplification to speak of. Nonetheless, we see cases of either low-frequency (IACM, NISR2) or high-frequency (VLS) amplifications up to 6-8. In addition to that, for SD>1.20, what one would perceive as the 'reference'

ground motion would depend very much on the orientation in which the sensor happened to be placed, since we see differences of up to factors of 2 or even 3 at certain frequencies. Figure A3 in the Supplement shows the directional dependence for all 60 stations of this study. Table A1 in the Supplement also includes columns related to the sensitivity (SD values and qualitative descriptions). Overall, considering all cases and comparing what appears strongly variable by visual inspection with the averaged SD values, we believe that a value less than 1.06 is rather low, higher than 1.15 is rather high, and higher than 1.20 is very high.

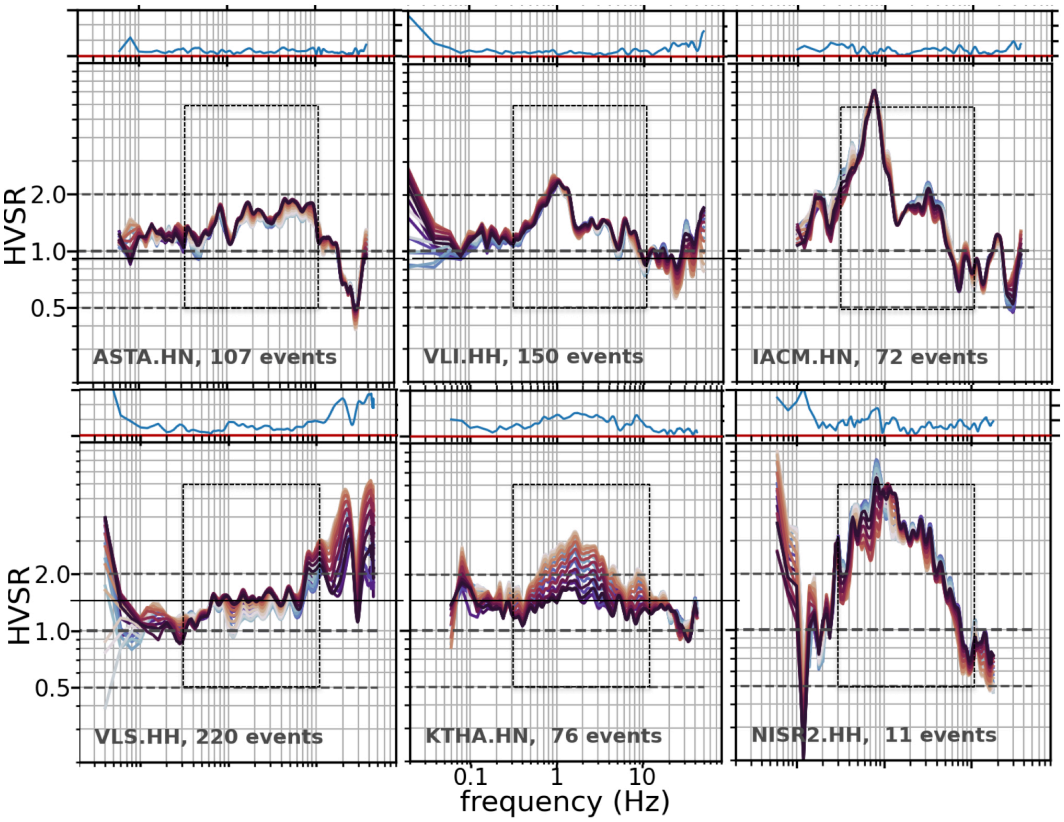

Figure 8: Indicative examples of HVSR: From left to right: low, medium and high amplification within the range of 0.3-10 Hz. From top to bottom, lower and higher variability with azimuth.

3.3 Correction of HVSR for the vertical component

We have noted that HVSR is but an underestimated proxy for the actual amplification level. To partially rectify that, we perform an additional calculation: we estimate the amended amplitude if we correct the HVSR for the implicit amplification of the vertical component. To do so, we use the function proposed by Ito et al. (2020) called VACF (correction function for vertical amplification). This has its limitations, since VACF was calibrated on Japanese data, but we consider it a not

illogical first approximation, coming from a region of similar (active) tectonic regime. VACF has been estimated by Ito et al. (2020) within a specific bandwidth, namely from 0.12-15 Hz, which is quite narrower than the typical bandwidth in this study. Hence, we do not venture to extrapolate beyond this field of applicability and constrain our corrections to the given range of applicability. We consider the corrected HVSR as an approximation of the standard spectral ratio (SSR) of Borcherdt (1970). An example comparison of HVSR and its VACF-corrected version is shown in Figure 10 for the two stations shown previously in Figure 4. For station APE (left), the 6-Hz resonant peak already identified by inspection of the mean HVSR becomes even more prominent after the VACF correction, with the amplification rising from 3 to 6. On the other hand, it is interesting to note that for station IMMV (right) –whose HVSR previously had not exhibited enough amplification to identify any significant peaks, and its response was considered passably flat- now a peak becomes visible at 1 Hz.

Figure A4 of the Supplement shows the comparison of HVSR and its VACF correction for all 60 stations of our dataset. This aims at giving a more realistic idea of potential amplification level within 15 Hz, but we note that these results are still approximations and carry the inherent potential shortcomings of HVSR, e.g., that an unexpected behaviour of the vertical component can map onto the predicted response of the horizontal. Table A1 in the Supplement includes A_{0_corr} (the maximum amplitude that the A_0 reaches if we correct the HVSR for the implicit amplification of the vertical component.), and in a few cases the newly identified resonant frequencies (f_{0_corr}) with their corresponding amplitude. We offer field A_{0_corr} in an indicative role, as a rough indication of the potential absolute amplification at the sites, and not to be used at face value for hazard or other calculations. We note that any very strongly nonlinear recordings (though this is not very probable for rock/stiff conditions) would be eliminated at the visual inspection stage, while weaker ones may still remain, since we assume they would not bias the ensemble mean results enough to merit a dedicated check. If present, we expect nonlinearity to decrease the level of high-frequency peaks. Since we are rather strict in our use of a threshold of 2 rather than 2.8 or 3, we believe it is not a grave issue.

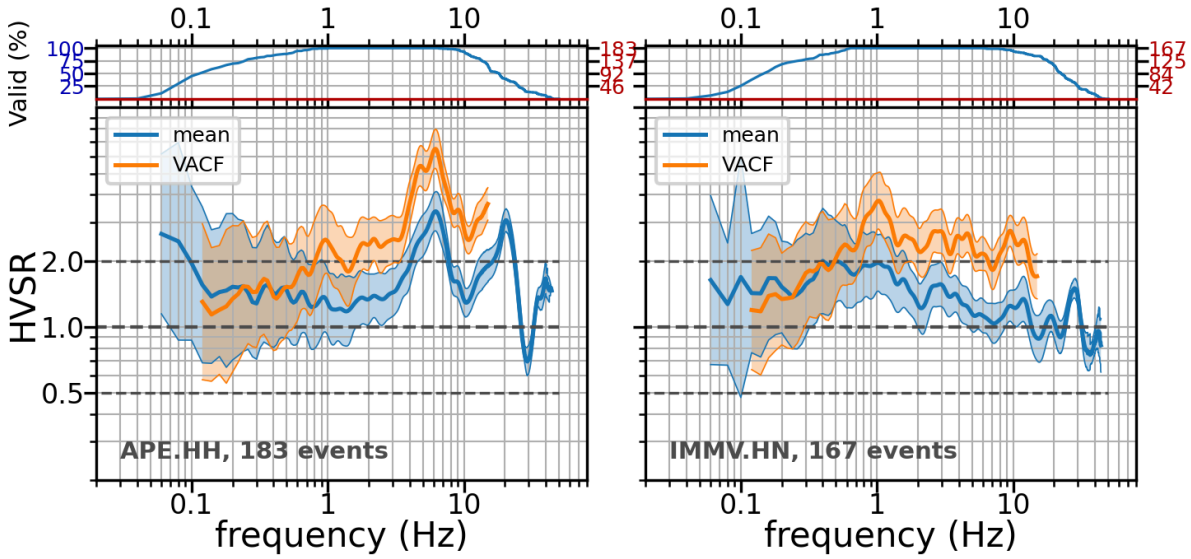

Figure 9: Comparison of mean HVSR ±1 SD (blue) with the corrected HVSR (orange) using Ito et al. (2020) correction function for the vertical component (VACF) at the same two stations shown in Figure 4. Left: an pre-existing peak is amplified. Right: a previously unidentified peak becomes visible.

3.3 Clustering

Now we consider the results across the ensemble of the 60 stations of this study and attempt to group them into a few indicative categories. To this end, we use hierarchical agglomerative clustering on the mean, orientation-independent HVSR. Agglomerative clustering starts by having each observation in its own cluster (of size 1), and builds a cluster hierarchy by iteratively merging the closest cluster-pair at each step. The resulting hierarchy (also called a dendrogram) is pruned at a suitable level either by defining a maximum inter-cluster distance, or by specifying the desired number of clusters. Agglomerative techniques are differentiated by the way they define the similarity (or linkage) between two clusters (i.e., sets of observations). For example, ‘complete’ linkage defines it as the maximum of all pairwise distances between participants of the two clusters, while ‘single’ linkage defines it as the minimum of such distances. In our case, after experimentation, we selected the Ward criterion (seeking to minimise the intra-cluster variance of the cluster that is being created) as the linkage method, while the Euclidean distance was used as a distance metric. The scikit-learn library was used for our experiments.

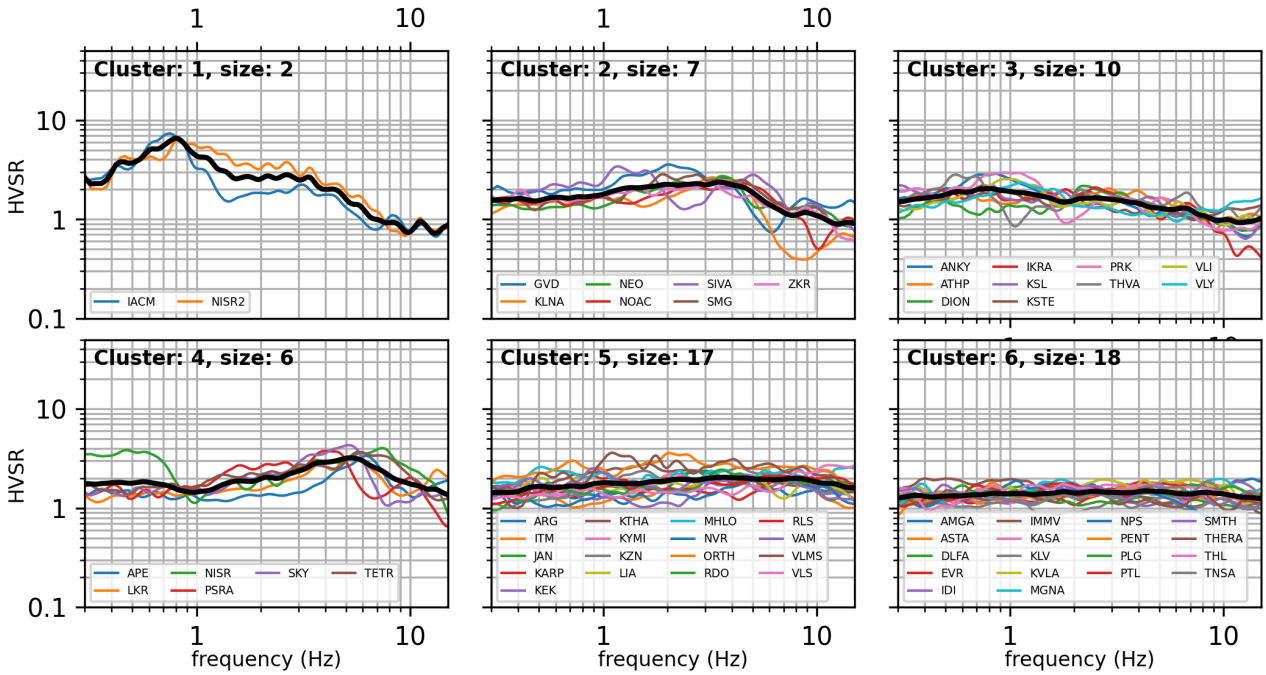

Figure 10: Groups of stations with similar amplification based on mean HVSR.

Figure 9 shows the six clusters derived from analysis of the HVSR curves. Cluster 1 shows clear low-frequency (LF) resonance for 2 sites, cluster 4 shows high-frequency (HF) amplification for 6 sites, and cluster 2 shows broadband amplification for 7 sites; all three categories would not be considered as optimal reference sites. Cluster 6 contains 18 reference sites. Clusters 3 and 5 show low amplification with a downtrending or flat shape respectively, so they could perhaps be acceptable reference sites. We repeat the clustering on the VACF-corrected HVSR and the results are shown in Figure 10, this time for 7 clusters. Although the cluster numbers change, many subgroups of stations maintain similar responses after VACF correction and are found together in new clusters after correction. Figure A5 of the Supplement compares the mean cluster shapes for the two cases. Table A1 of the Supplement includes the cluster number per station according to both groupings, and a qualitative description. The main classes identified by this analysis can be roughly distinguished as: reference stations, LF/HF/broadband amplification that makes the response deviate from a reference site, and smaller amplification patterns that do not deviate strongly from flat response. Other groupings could be reached by constraining the algorithm parameters, but our goal here is to call attention to a few patterns and how/if they deviate from the expected (flat) rock response.

We do not investigate on a station-by-station basis what exactly lies behind the amplification patterns we observe. Considering these are generally thought to be rock sites, in what follows we only mention a few possible interpretations (other than geological misclassification). It is known that sharp high-frequency peaks can be due to shallow, near-surface soft or weathered layers on bedrock. Their level will increase with the impedance (Vs) contrast between the two materials. A

directional dependence of such a peak could signify 2D or 3D effects stemming from non-horizontal conditions. A low-frequency, relatively low peak could indicate a deep interface, likely between soft and harder rock. A high-frequency frequency can indicate shallow weathered rock over rock (Ktenidou, 2022). Given the hardness of the sites, another likely physical mechanism is topographic amplification, which would be expected to take place at specific frequencies, depending on the overall material Vs and the height/width of the hill/slope/topographic feature (Geli et al., 1988; Ashford & Sitar, 1997). In this case, the spectral peak will also exhibit directionality, since such amplification is known to be strongest in a certain direction, such as transversely to the axis of a 2D ridge. We expect the interpretation to be more complex in the case of a 3D feature such as a hill or cave (instances of which exist in our database, see next section). We also mention that in the cases of volcanic structures, additional complexity can also be expected.

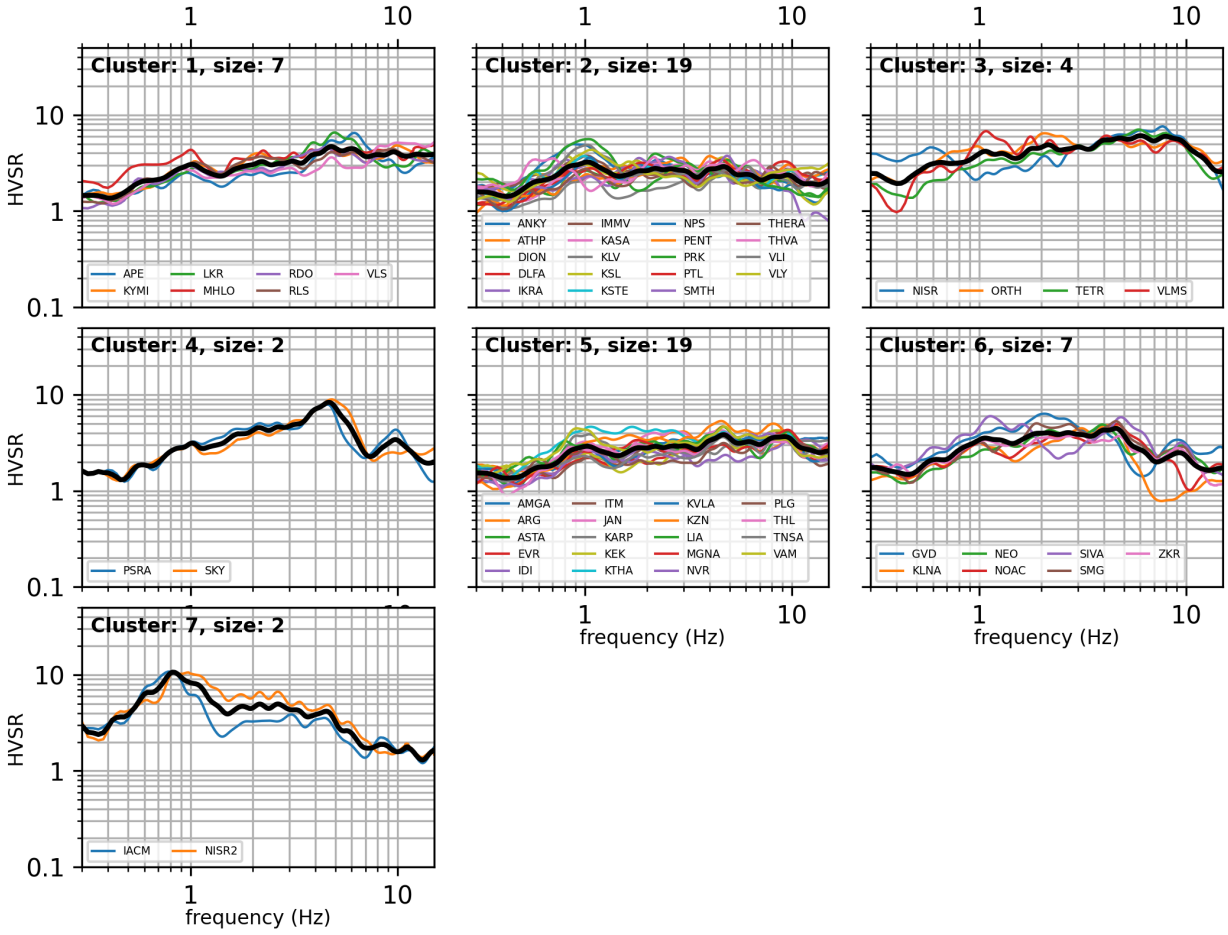

Figure 10: Groups of stations with similar amplification based on mean VACF-corrected HVSR.

Table A1 of the Supplement compiles all the data-derived results estimated in this section, such as: f_0, A_0, f_1, A_1 (if applicable), f_{0_corr} A_{0_corr}, $SD_{0.3\text{-}30}$, $SD_{1\text{-}10}$, SD_{fo}, directionality qualifiers, cluster numbers, and description of amplification pattern. Table A1, along with all tables, is available in xls format as supplementary material (assets).

We note here, at the end of the HVSR section, that it is out of the scope of this paper to present comparisons of HVSR at collocated stations, i.e., compare the HH and HN results in cases where both are available. This was done at a preliminary stage and it helped identify a small number of component or metadata issues which were since corrected. Although it is expected that the high-frequency part of the HVSR may differ due to the precise installation conditions (see also the dedicated section 3.3), the salient characteristics for our stations were the same. We choose to show results from the HN sensors (marked HNc in Table 1) because they have the benefit of not clipping, and hence allow for a richer dataset for this particular study, which consists of the stronger recordings available.

3 Compiling other station metadata

3.1 Suggested parameter schemes for station classification

There have been several studies and projects dedicated to assessing the most useful parameters and proxies when it comes to describing site conditions at a station, each of them using different methods across different scales. We mention some well-known and recent ones below:

a. Cultrera et al. (2021) conducted a wide European survey including various end users and considering aspects such as cost and difficulty in procuring the parameters, which concluded that the preferred 7 indicators out of a total of 24 –some being admittedly not very common- are the following: 1. fundamental frequency f_0; 2. full Vs profile; 3. Vs_{30}; 4. depth to seismological bedrock; 5. depth to engineering bedrock; 6. surface geology; and 7. soil class. We note that some of these are direct derivatives of others (3 hinging upon 2 and 7 depending on 2 and 4).

b. Lanzano et al. (2020) conducted a study in Central Italy focusing on rock sites in particular, and proposed an algorithm that takes into account 6 site descriptors, grading and combining them mathematically to produce an overall qualifier for characterising reference stations. Their proxies used to identify rock stations are: 1. housing/installation conditions; 2. topographic conditions; 3. surface geology (same as 6 above); 4. Vs_{30} (same as 3 above); 5. shape of HVSR from noise or earthquakes (related to 1 above); 6. δs2s, the site-to-site term resulting from GMPE residuals analysis using response spectra, as an alternative estimate of the transfer function.

c. Pilz et al. (2020) assess reference stations at a European level from homogenized data considering the following parameters: 1. surface geology (as above); 2. slope/topography (as above); 3. HVSR (as above); 4. similarity of surface κ_0 (high-frequency site attenuation; Anderson and Hough, 1984; Ktenidou et al., 2014) to coda κ_0, which is considered as indicative of deeper conditions; 5. ML station residuals.

3.2 Rationale and selected parameters for this study

In the previous section we computed FAS-based HVSR for the first time for our stations, providing a first set of data-derived parameters that can help characterize seismic site response at our stations. These went beyond the typical outcomes of fundamental frequency f_0 or shape of HVSR, which were mentioned in the schemes above. Our analyses examined HVSR at some depth and yielded metrics not typically considered, such as directional sensitivity in different frequency bands, amplitude correction, etc. On the other hand, there are other data-derived parameters mentioned in the schemes above that we do not attempt to assess in this study, namely δs2s and κ_0. In the case of δs2s, to avoid trade-offs between station and events residuals, the data distribution needs to be appropriate including as many recordings as possible per event (we only have a limited number for most cases), and even so because it works on specific pre-selected oscillator periods and in the response spectral domain, the results are not always as detailed as FAS-based analysis. In the case of κ_0. to avoid the classic trade-offs between near-surface and path attenuation, the distance distribution needs to be appropriate, which is not the case in many stations, and especially at HH ones. Hence such data-based techniques are not considered at this time. With an appropriate set of κ0 estimates for the 60 rock candidate sites, the lowest values could be prioritized as potential reference stations, as in the case of Morasca et al. (2023).

To the HVSR-derived parameters computed above, we now prepare to add any available additional descriptors we can find that are not derived by seismic data. Many of these come from external sources, namely publications, databases, websites and maps. Others come from internal sources, i.e. the insider's knowledge that only an operator has. The parameters we choose to compile are: housing/installation, topography/slope, surface geology, and Vs_{30}. We remind the reader that ad-hoc Vs profiles are almost non-existent in Greek seismic stations, and thus parameters such as full Vs profile and depths to seismological or engineering bedrock are not readily available. On the other hand, we do not opt for EC8 site class as a parameter to collect, as this is not independent but relies on others.

We believe it is of paramount importance to go beyond a 'literature-based' collation and add insights based on site visits by NOA personnel. We believe this is important because geological maps constructed for an entire country inevitably contain errors and simplifications, whereas a site walkover of the station location by an experienced geologist provides additional reliability. Similarly, satellite-based estimates of slope/topography invariably include approximation, homogenisation and some lack of specificity depending on the size of the 'pixel', whereas again a site visit laves little doubt as to the exact nature of the landscape at the station.

3.3 Station installation

Installation conditions have been known since the early observations of Cranswick et al. (1984) to affect seismic recordings especially at high frequencies, and this discussion has revived recently (Hollender et al., 2020; Castellaro et al., 2022). Table A2 of the Supplement compiles the information we found on housing and installation conditions at our 60 rock stations. Information for the HN stations is available from the website https://accelnet.gein.noa.gr/station-information/ (last accessed:

December 2023), while additional detail specially for the HH stations is provided by the operator based on site visits, with more detailed descriptions given in the dedicated article on EIDA@NOA (Evangelidis et al., 2021). The last column of the table provides our assessment as to whether each station can be considered a reference station based on installation conditions. We note here that housing conditions for HL network are vastly different to those of other countries, with explicit free-field conditions being rather rare. The Italian equivalent (Lanzano et al., 2020) only makes reference to two types of stations, free-field and in power towers, while the NOA network has had to make use of environments as diverse as monastery cells. However, in all cases where a 'vault' is mentioned, this is created within the structure hosting it by cutting around the station in a way so as to isolate its potential motion from that of the surrounding structure, hence avoiding soil-structure interaction effects.

3.4 Topography and slope

Table A3 compiles the information gathered on terrain slope and topographic conditions at our stations. There are various sources. For the HN stations, ESM (https://esm-db.eu/; Lanzano et al., 2021; Luzi et al., 2016) provide the slope in degrees along with their classification into four categories with the following code: T1: 'Flat surface, isolated slopes and cliffs with average slope angle i≤15°'; T2: 'Slopes with average slope angle i>15°'; T3: 'Ridges with crest width significantly less than the base width and average slope angle 15°≤i≤30°'; T4: 'Ridges with crest width significantly less than the base width and average slope angle i>30°'. For the HN stations again, Margaris et al. (2021) provide an estimate of slope which we have also converted into degrees and which for the most part almost coincides with the angles by ESM (save 2 stations marked in the table in bold italics, DLFA and NOAC, where however the difference does not cause a change in ESM code). Despite this effort to collect information on the geomorphology at the stations from external sources, which have the advantage of being homogeneous across a larger scale, we believe that on a site-specific basis the most reliable and precise information comes from the operator based on site visits. Thus, for the entirety of stations studied, additional detail is also provided in Table A3 based on site visits, where we group stations into the following categories: 1. Flat/shallow (<15) within 200 m; 2. Steep (<30) within 200 m; 3. Steep hill crest; 4. Near cliff. This offers new information for about 35 stations for which no information was available before, some of them on various kinds of steep conditions.

3.5 Vs_{30}

Table A4 compiles the information gathered on Vs at our study's rock stations. There are again various sources. For the HN stations, ESM again provides the proxy-based Vs_{30} using slope (and consequent EC8 soil class as per CEN, 2004), while Margaris et al. (2021) provide a variety of estimates of Vs_{30}. A couple come from measurements in the vicinity of the stations (within 1 km, as per Stewart et al., 2014), while most are derived from proxies, using not only ground slope but also terrain, and a single value per station is given as preferred by that study. We note that although Stewart et al. (2014) was based on entire Vs profiles, that study did not release any profiles as functions of depth, but rather their derived average Vsz values over a given depth z. Finally, a couple of stations have been characterised ad hoc at the station location by NOA

within the national project HELPOS (Deliverable 2.5.3, Geophysical measurements at seismic stations). Between the three sources of information, namely ESM, Margaris et al. (2021) and HELPOS, there are in some cases discrepancies. The strongest contradictions that correspond to, say, a factor of 2-3 of difference in Vs_{30} and a clear jump in site class, are marked in Table A4 in bold italics, such as ATHP, IACM, KASA, KSL, SMTH. In the case of measured Vs profiles on the spot (HELPOS), we consider those as the definitive Vs_{30} estimates. On the contrary, in the case of measurements within 1 km distance form the station, we believe their validity very much depends on lateral variations in stratigraphy, and so we do not attach more confidence to them than the proxy-based ones of ESM.

3.6 Geology

Table A5 compiles all the information gathered on surface geology at our study's rock stations. Information for the HN stations is available from the website https://accelnet.gein.noa.gr/station-information/ (last accessed: December 2023). Description of the geological unit and age are provided for HN stations by Margaris et al. (2021). Finally, 17 of our 60 stations were also found in the list of Pilz et al. (2020) for European reference sites, and in those cases we also report the unified geological descriptors attributed by them according to the European Geological Data Infrastructure (EGDI). Two of those attributes were based on AI and are noted as such in the table.

One of the important features of this study is that we provide new information for the entirety of stations, consisting of geological unit and age descriptions. This is based on the combination of site visit and walkover experience with the detailed revisiting of maps and literature. The majority of stations were located in 53 geological maps (1:50,000 scale) published by the Hellenic Survey of Geology and Mineral Exploration (HSGME) and their geology interpreted in conjunction with knowledge of the local features from sit visits. Geological conditions for a couple of stations were derived from relevant publications indicated in Table A5 with an asterisk. There are several contradictions between the various sources, too numerous to discuss in detail here. Our best estimate after assessing all available information and experience is given in the relevant columns 'this study'.

Table 2. Compilation of reference site potential per station according to each criterion, and final disposition resulting from co-assessment.

No.	Station code	Installation	Topography	Vs_{30}	Geology	HVSR - shape & level	HVSR - Directionality	Final disposition
1	AMGA	no	yes	no	yes	yes	yes	very good
2	ANKY	no	yes	yes - ESM	likely	ok	yes	good
3	APE	yes	yes	-	yes	no	not > 10 Hz	good < 10 Hz
4	ARG	yes	yes	no	no	ok	no	
5	ASTA	no	yes	yes - ESM	no	yes	yes	very good
6	ATHP	no	yes	yes - Helpos	no	ok		
7	DION	no	yes	no	yes	ok		
8	DLFA	no	no	yes - ESM	yes	yes	yes	very good
9	EVR	yes	yes	-	yes	yes		very good
10	GVD	yes	yes	no	no	no	yes	ok
11	IACM	yes	yes	no	likely	no		

12	IDI	yes	no	-	yes	yes		ok
13	IKRA	no	yes	no	yes	ok		
14	IMMV	no	yes	yes - ESM	no	yes		ok
15	ITM	yes	yes	yes - ESM	no	ok		good
16	JAN	yes	yes	no	no	ok		good
17	KARP	yes	no	yes - ESM	yes	ok	yes	very good
18	KASA	no	no	yes - ESM	yes	yes		ok
19	KEK	yes	no	-	yes	ok	no	
20	KLNA	no	yes	no	no	no		no
21	KLV	no	no	-	yes	yes	yes	ok
22	KSL	yes	no	yes - ESM	yes	ok	no	good
23	KSTE	yes	no	-	yes	ok		
24	KTHA	no	no	no	yes	ok	no	no
25	KVLA	no	yes	yes - ESM	yes	yes	yes	preferred
26	KYMI	yes	no	yes - ESM	yes	ok	no	good
27	KZN	yes	yes	no	yes	ok	no	good
28	LIA	no	yes	no	yes	ok		
29	LKR	yes	yes	-	no	no	no	no
30	MGNA	no	yes	no	yes	yes		ok
31	MHLO	no	yes	-	no	ok		no
32	NEO	yes	yes	-	yes	no		ok
33	NISR	no	no	-	yes	no	no	no
34	NISR2	yes	no	-	yes	no	no	no
35	NOAC	yes	yes	no	yes	no		ok
36	NPS	yes	yes	-	yes	yes	not > 10 Hz	very good < 10 Hz
37	NVR	yes	yes	yes - ESM	yes	ok	yes	preferred
38	ORTH	no	yes	-	yes	ok		
39	PENT	no	no	-	no	yes		no
40	PLG	yes	yes	no	yes	yes	yes	preferred
41	PRK	yes	yes	no	yes	ok		good
42	PSRA	no	yes	no	yes	no	yes	ok
43	PTL	yes	yes	-	yes	yes		very good
44	RDO	yes	yes	-	yes	ok		good
45	RLS	yes	yes	-	likely	ok		ok
46	SIVA	yes	yes	no	yes	no		ok
47	SKY	no	no	-	yes	no		no
48	SMG	yes	yes	no	yes	no		ok
49	SMTH	yes	no	yes - ESM	yes	yes	yes	preferred
50	TETR	yes	no	-	yes	no	not > 10 Hz	
51	THERA	yes	no	-	yes	yes	no	ok
52	THL	yes	yes	-	yes	yes	yes	preferred
53	THVA	no	yes	-	no	ok		no
54	TNSA	no	yes	no	yes	yes		ok
55	VAM	yes	yes	-	yes	ok	no	good
56	VLI	yes	yes	-	yes	ok	yes	very good
57	VLMS	yes	yes	no	yes	ok		good
58	VLS	yes	yes	yes - Marg21	no	ok	not > 10 Hz	very good < 10 Hz
59	VLY	yes	yes	-	yes	ok		good
60	ZKR	no	yes	yes - Marg21	yes	no		ok

525

4 Discussion and conclusions

In the previous sections, we compiled several descriptors for our stations and derived amplification characteristics from our strong-motion data analysis. We now bring everything together in Table 2 to co-evaluate the overall potential of our stations as reference stations. We take into account all criteria, in a transparent way, challenging all parameters by openly contrasting them with all others. We do not attribute numerical values and weights to each parameter, as is done e.g. in the summation rationale of Lanzano et al. (2021). We believe there are inherent issues with quantifying qualitative data and treating them as

homogeneous to perform mathematical operations between them. Moreover, our goal is not to provide a continuous ranking across all sites. We opt for co-assessing all input and offering an overall qualitative assessment of reference site potential. In Table 2 we consider stations that got a positive assessment in 6 factors as 'preferred' reference sites (5 instances), those who missed 1 field as 'very good' (9 instances) those that missed 2 or 4 fields as 'good' or 'ok', noting bandwidth. Stations that ranked lower are not generally recommended, though the user can select them for specific purposes or within specific frequency bands according to her/his own judgement. Different schemes could be contrived to evaluate and even prioritise the stations, but we do not feel an absolute grading is necessary, especially since the appropriateness will also depend on the precise nature of the application making use of the reference motion. It is a strong message for us to convey that over half the stations did not rank as reliable enough reference stations, and we feel that more work is needed to reassess the implications of this finding. It is also interesting to note that some of our rock sites had high-frequency amplifications: this is in line with the definition of A-class sites in EC8, which is shifting from the current version (CEN, 2004) of Vs_{30}>800 m/s, to a new version (Labbé and Paolucci, 2022) where there is also a provision of f_0>10 Hz.

In this study, we compute FAS-based HVSR for the first time for all the HL rock stations, producing a rich suite of metadata that greatly exceeds the outcomes of typical HVSR analysis (f_0). We also compile all existing parameters we can find from various sources (housing/installation, topography/slope, surface geology, and Vs_{30}; ad-hoc Vs profiles being almost non-existent across Greek seismic rock stations). We compare and contrast those metadata from various sources and, in addition, we offer insights and corrections based on site visits from a network operator's point of view. We believe this operator's first-hand experience is very important because geological maps constructed at such a scale as to serve an entire country (and made by different teams, over several decades) inevitably contain errors and simplifications, whereas a site walkover of the station location by an experienced geologist provides additional reliability. Similarly, satellite-based estimates of slope/topography invariably include approximation, homogenisation and some lack of specificity depending on the size of the 'pixel', whereas again a site visit leaves little doubt as to the exact nature of the landscape at the exact location of the station. The information for rock stations up to now has been sparse and scattered for the strong-motion case, and almost nonexistent for the broadband one. Until now, if a user wished to select a reference station in the HL network, s/he might have resorted to geology, or even considered all rock stations as interchangeable. We hope this work has provided the first step towards a better evaluation of rock stations and eventually towards the better utilisation of their data. We believe this work is in line with the user needs already identification in literature, e.g. by Zhu et al. (2020), who asked of all network operators to open and share not only f0 values but preferably their entire amplification functions. To the extent of enriching typical HVSR methodology in 3 ways (exhausting usable bandwidth, correcting for vertical and investigating directionality), we think that the outcomes exceed what has been asked. Moreover, by compiling all other kinds of literature-, map- and operator-derived information, we offer the user transparency to all criteria and the possibility to prioritise and tailor them to their individual needs. Until now, a user might likely select a reference station from the HL based on a single source of information, which would carry much larger risks with respect to using our collation of parameters. And we have shown that the selection process matters, since not all rock sites should be treated equally or trusted blindly.

Finally, we believe that data-derived transfer functions are extremely important and illuminating for understanding station response. There is sometimes a fixation on Vs_{30} which is not only inadequate (too shallow, and providing no indication of impedance depth or contrast), but may even be unnecessary if we have both the geology and –what is more- the empirical site response from recordings. Even a full Vs profile may be inadequate to fully assess site response, if we consider that its high-frequency part depends heavily on the assumptions we made of damping, and –most of all- that its premise for yielding reliable site response is that the 1D assumption holds true, which in nature is rarely the case (and especially perhaps for rock sites - whereas empirical estimates of site effects, may have their shortcomings but reflect the 3D nature of the formations). Our study has shown once again that not all 'rock' sites should be treated -or trusted- equally. Also, we would ask the question: if we have data-derived site response, how much importance should stand-alone meta-descriptors and proxies such as Vs_{30} be given?

Data availability

All waveforms and station metadata were downloaded and are freely accessible at https://eida.gein.noa.gr/, the regional node of EIDA (the European Integrated Data Archive) hosted by the Institute of Geodynamics of the National Observatory of Athens (NOA). Data from NOA's seismic network bear the network code HL and are attributed DOI:10.7914/SN/HL (NOA-GI, 1975). Event parameters come from the seismic catalogue of NOA, freely accessible here: https://eida.gein.noa.gr/fdsnws/availability/1. Station metadata come from the various articles cited in the paper, as well as the ESM (https://esm-db.eu/; Lanzano et al., 2021; Luzi et al., 2016). Maps published by the Hellenic Survey of Geology and mineral Exploration are generally available by HSGME for purchase, and hence not freely accessible.

Author contribution

OJK had the idea, coordinated the team, and wrote the paper. AP performed manual data processing and final data check and curated the database. EVP performed the main coding and calculations. ZC compiled and interpreted the ground motion station metadata. FG performed initial curation, quality assessment and manual data processing. FC performed manual data processing. SL contributed the geological interpretations and oversaw PS and KF in compiling the geological station metadata. CPE provided insights on station history, installation and performance.

Competing interest

The contact author has declared that none of the authors has any competing interests.

Acknowledgements

Discussions with several colleagues have helped the lead author since she joined NOA in 2018; among others, Ioannis Kalogeras, Thymios Sokos, Hiroshi Kawase, Laurentiu Danciu and Alexis Chatzipetros are cordially thanked in order of appearance. The authors thank the two referees, Giovanni Lanzano and Chuanbin Zhu, as well as the associate editor and community comments for their useful comments and suggestions. No funding is acknowledged, except the small internal scholarship 'ROAR' awarded by NOA to OJK. Some plots were created using Generic Mapping Tools (GMT; Wessel et al. 2013) and the help of this fantastic tool is cordially acknowledged. Finally, no AI was used in developing this manuscript - we used what human intelligence was available.

References

Ancheta, T.D., R.B. Darragh, J.P. Stewart, E. Seyhan, W.J. Silva, B.S.-J. Chiou, K.E. Wooddell, R.W. Graves, A.R. Kottke, D.M. Boore, T. Kishida, J.L. Donahue, NGA-West2 Database, Earthquake Spectra, 30(3), 989–1005. doi: https://doi.org/10.1193/070913EQS197M, 2014.

Anderson, J.G, S.E. Hough, A model for the shape of the fourier amplitude spectrum of acceleration at high frequencies, Bull. Seismol. Soc. Am., 74 (5): 1969–1993. doi: https://doi.org/10.1785/BSSA0740051969, 1984.

Ashford, S.A. and Sitar N.: Analysis of Topographic Amplification of Inclined Shear Waves in a Steep Coastal Bluff, Bull. Seism. Soc. Am., 87, 692-700, DOI: 10.1785/BSSA0870030692, 1997.

Borcherdt, R. D.: Effects of local geology on ground motion near San Francisco Bay, Bull. Seismol. Soc. Am., 60, 29–61, 1970.

Brune, J.N.: Tectonic stress and the spectra of seismic shear waves from earthquakes, J. Geoph. Res., 75, 4997–5002, 1970.

Brune, J.N.: Correction to 'Tectonic stress and the spectra, of seismic shear waves from earthquakes, J. Geoph. Res., 76, 5002, 1971.

Castellaro, S., Alessandrini, G., & Musinu, G.: Seismic station installations and their impact on the recorded signals and derived quantities. Seis. Res. Lett., 93(6), 3348-3362, https://doi.org/10.1785/0220220029, 2022.

CEN (Comité Européen de Normalisation): Eurocode 8: Design of structures for earthquake resistance. Part 1: general rules, seismic actions and rules for buildings (EN 1998–1: 2004), Brussels, Belgium, 2004.

Crowley H., Dabbeek J., Despotaki V., Rodrigues D., Martins L., Silva V., Romão, X., Pereira N., Weatherill G. and Danciu L., European Seismic Risk Model (ESRM20), EFEHR Technical Report 002, V1.0.0, https://doi.org/10.7414/EUC-EFEHR-TR002-ESRM20 (2021)

Cultrera, G., Cornou, C., Di Giulio, G. and Bard, P.Y.: Indicators for site characterization at seismic station: recommendation from a dedicated survey, Bull. Earth. Eng. 19 (11), 4171-4195, DOI: 10.1007/s10518-021-01136-7, 2021.

Danciu L., Nandan S., Reyes C., Basili R., Weatherill G., Beauval C., Rovida A., Vilanova S., Sesetyan K., Bard P-Y., Cotton F., Wiemer S., Giardini D., The 2020 update of the European Seismic Hazard Model: Model Overview, EFEHR Technical Report 001, https://doi.org/10.12686/a15 (2021)

Di Giulio, G., Cultrera, G., Cornou, C., Bard, P.Y., Tfaily, B.Al.: Quality assessment for site characterization at seismic stations, Bull. Earth. Eng.,19 (12), 4643-4691, doi:10.1007/s10518-021-01137-6, 2021.

Evangelidis, C.P., Triantafyllis, N., Samios, M., Boukouras, K., Kontakos, K., Ktenidou, O-J. and 32 others: Seismic waveform data from Greece and Cyprus: Integration, archival and open access, Seismol. Res. Letts, 92, 1672–1684, doi:10.1785/0220200408, 2021.

Geli, L., Bard P.Y. and Jullien B.: The effect of topography on earthquake ground motion: a review and new results. Bull. Seism. Soc. Am. 78, 42-63, 1988.

Goulet, C., Kishida, T., Ancheta, T.D., Cramer, C.H., Darragh, R.B., Silva, W.J., Hashash, Y.M.A., Harmon, J., Stewart, J.P., Wooddell, K.E. and Youngs, R.R.: PEER NGA-East database. PEER Report 2014/17, Berkeley, CA: Pacific Earthquake Engineering Research Center, 2014.

Grendas, I., Theodoulidis, N., Hatzidimitriou, P., Margaris, B. and Drouet, S.: Determination of source, path and site parameters based on non-linear inversion of accelerometric data in Greece, Bull. Earth. Engin., doi:10.1007/s10518-018-0379-8, 2018.

Hollender, F., Roumelioti, Z., Maufroy, E., Traversa, P., & Mariscal, A.: Can we trust high-frequency content in strong-motion database signals? Impact of housing, coupling, and installation depth of seismic sensors. Seis. Res. Lett., 91(4), 2192-2205, https://doi.org/10.1785/0220190163, 2020.

Institute of Engineering Seimology Earthquake Engineering - ITSAK (1981). ITSAK Strong Motion Network [Data set]. International Federation of Digital Seismograph Networks. https://doi.org/10.7914/SN/HI

Ito, E., Nakano, K., Nagashima, F. and Kawase H.: A Method to Directly Estimate S-Wave Site Amplification Factor from Horizontal-to-Vertical Spectral Ratio of Earthquakes (eHVSRs), Bull. Seismol. Soc. Am., 110, 2892–2911, doi: 10.1785/0120190315, 2020.

Kishida, T., Ktenidou, O-J., Darragh, R. and Silva, W.: Semi-automated procedure for windowing time series and computing Fourier Amplitude Spectra (FAS) for the NGA-west2 database. PEER report 2016/02, Berkeley, CA: Pacific Earthquake Engineering Research Center, 63, 2016.

Konno, K. and Ohmachi, T.: Ground-motion characteristics estimated from spectral ratio between horizontal and vertical components of microtremor. Bull. Seismol. Soc. Am., 88(1), 228–241, https://doi.org/10.1785/BSSA0880010228, 1998.

Ktenidou, O.-J., F. Cotton, N.A. Abrahamson, J.G. Anderson, Taxonomy of κ: A Review of Definitions and Estimation Approaches Targeted to Applications. Seismol. Res. Letts, 85(1), 135–146, doi: https://doi.org/10.1785/0220130027, 2014.

Ktenidou, O.-J. and Abrahamson, N.: Empirical estimation of high-frequency ground motion on hard rock. Seismol. Res. Letts, 87, 1465–1478, DOI: 10.1785/0220160075, 2016.

Ktenidou, O.-J., Kalogeras, I.: The accelerographic network of the National Observatory of Athens, Greece: improving site characterisation using strong motion recordings, 2nd International Conference on Natural Hazards & Infrastructure (ICONHIC), Chania, 23-26 Jun, 2019.

Ktenidou, O.-J.: Hard as a rock? Reconsidering rock-site seismic response and reference ground motions. In: Progresses in European Earthquake Engineering and Seismology - Third European Conference on Earthquake Engineering and Seismology – Bucharest, 2022, Ed. R. Vacareanu & C. Ionescu, Springer Proceedings in Earth and Environmental Sciences, https://doi.org/10.1007/978-3-031-15104-0_3 , 2022.

Ktenidou, O.-J., Chávez-García, F.J., Raptakis, D. and Pitilakis, K.D.: Directional dependence of site effects observed near a basin edge at Aegion, Greece, Bull. Earth. Eng., 14(3), 623-645, doi:10.1007/s10518-015-9843-x, 2016.

Ktenidou, O.-J., Gkika, F. and Evangelidis, C.: The Quest for Rock Site Characterization for the Greek National Seismic Network, EUROENGEO: 3rd European Regional Conference of IAEG, Athens/online, 6-9 Oct, 2021a.

Ktenidou, O.-J., Gkika, F., Pikoulis, E.V. and Evangelidis, C.: Hard as a rock? Looking for typical and atypical reference sites in the Greek network, EGU General Assembly (online), 19-30 Apr., DOI:10.5194/egusphere-egu21-13659, 2021b.

Labbé, P. and Paolucci, R.: Developments Relating to Seismic Action in the Eurocode 8 of Next Generation. In: Progresses in European Earthquake Engineering and Seismology - Third European Conference on Earthquake Engineering and Seismology – Bucharest, 2022, Ed. R. Vacareanu & C. Ionescu, Springer Proceedings in Earth and Environmental Sciences, 2022.

Lanzano, G., Luzi, L., Cauzzi, C., Bienkowski, J., Bindi, D., Clinton, J., Cocco, M., D'Amico, M., Douglas, J., Faenza, L., Felicetta, C., Gallovic, F., Giardini, D., Ktenidou, O-J. and 12 others: Accessing European Strong-Motion Data: An Update on ORFEUS Coordinated Services, Seismol. Res. Letts, 92, 1642–1658, doi:10.1785/0220200398, 2021.

Lanzano, G., Felicetta, C., Pacor, F., Spallarossa, D. and Traversa, P.: Methodology to identify the reference rock sites in regions of medium-to-high seismicity: An application in Central Italy, Geophys. J. Int., 222, 3, 2053–2067, DOI: 10.1093/gji/ggaS261, 2020.

Lanzano, G., Felicetta, C., Pacor, F., Spallarossa, D. and Traversa, P.: Generic-To-Reference Rock Scaling Factors for Seismic Ground Motion in Italy, Bull. Seismol. Soc. Am. XX, 1–24, doi: 10.1785/0120210063, 2022.

Lermo, J., and Chavez-Garcia, F.G.: Site effect evaluation using spectral ratios with only one station, Bull. Seismol. Soc. Am., 83,1574–1594, 1993.

Luzi, L., Puglia, R., Russo, E., D'Amico, M., Felicetta, C., Pacor, F., Lanzano, G., Çeken, U., Clinton, J., Costa, G., Duni, L., Farzanegan, E., Gueguen, P., Ionescu, C., Kalogeras, I., Özener, H., Pesaresi, D., Sleeman, R., Strollo, A. and Zare, M.: The engineering strong motion database: A platform to access pan-European accelerometric data, Seismol. Res. Letters, 87(4), 987–99, DOI: 10.1785/0220150278, 2016.

Margaris, B.E., Scordilis, M., Stewart, J.P., Boore, D.M., Theodulidis, N., Kalogeras, I., Melis, N., Skarlatoudis, A., Klimis, N. and Seyhan, E.: Hellenic strong-motion database with uniformly assigned source and site metadata for period of 1972-2015, Seismol. Res. Letts, 92, 2065-2080, doi: 10.1785/0220190337, 2021.

Margaris, B., Kalogeras, I., Papaioannou, Ch., Savvaidis, A. and Theodoulidis, N.: Evaluation of the national strong motion network in Greece: Deployment, data processing and site characterization, Bull. Earth. Engin., 12, 237 - 254, https://doi.org/10.1007/s10518-013-9580-y, 2014.

Meinhold, G., D. Kostopoulos, T. Reischmann: Geochemical constraints on the provenance and depositional setting of sedimentary rocks from the islands of Chios, Inousses and Psara, Aegean Sea, Greece: implications for the evolution of Palaeotethys. Journal of the Geological Society, 164 (6), 1145–1163. doi: https://doi.org/10.1144/0016-76492006-111, 2007

Morasca, P., D'Amico, M., Sgobba, S., Lanzano, G., Colavitti, L., Pacor, F., & Spallarossa, D.: Empirical correlations between an FAS non-ergodic ground motion model and a GIT derived model for Central Italy. Geophysical Journal International, 233(1), 51-68, https://doi.org/10.1093/gji/ggac445, 2023.

National Observatory of Athens, Institute of Geodynamics, Athens – NOA-GI (1975). National Observatory of Athens Seismic Network [Data set]. International Federation of Digital Seismograph Networks. https://doi.org/10.7914/SN/HL

Pilz, M., Cotton, F. and Reddy Kotha, S.: Data-driven and machine learning identification of seismic reference stations in Europe, Geoph. J. Int., 222, 2, 861–873, https://doi.org/10.1093/gji/ggaa199, 2020.

Pitilakis, K., Riga, E., Apostolaki, S., Danciu, L.: Seismic hazard zonation map and definition of seismic actions for Greece in the context of the ongoing revision of EC8, Bull. Earthq. Eng., 22, 3753–3792, https://doi.org/10.1007/s10518-024-01919-8, 2024.

Puglia, R., Albarello, D., Gorini, A., Luzi, L., Marcucci, S. & Pacor, F. Extensive characterization of Italian accelerometric stations from single-station ambient-vibration measurements, Bull. Earthq. Eng., 9, 1821–1838, https://doi.org/10.1007/s10518-011-9305-z, 2011.

Silva, W.J. and Darragh, R.: Engineering Characterization of Earthquake Strong Ground Motion Recorded at Rock Sites (TR-102261), Palo Alto, CA: Electric Power Research Institute. Available at: https://www.epri.com/research/products/TR-102262, 1995.

Steidl, J.H., Tumarkin, A.G. and Archuleta, R.J: What is a reference site? Bull. Seism. Soc.Am., 86(6), 1733-1748, DOI: 10.1785/BSSA0860061733, 1996.

Stewart, J.P., Klimis, N., Savvaidis, A., Theodoulidis, N., Zargli, E., Athanasopoulos, G., Pelekis, P., Mylonakis, G. and Margaris, B.: Compilation of a local VS profile database and its application for inference of VS30 from geologic and terrain - based proxies, Bull. Seism. Soc. Am., 104, 2827 - 2841, https://doi.org/10.1785/0120130331, 2014.

Theodoulidis, N., Kalogeras, I., Papazachos, C.B., Karastathis, V., Margaris, B.N., Papaioannou, Ch., Skarlatoudis A.A.: HEAD v1.0: A unified Hellenic Accellerogram Database, Seis. Res. Lett., 75, 36 - 45, 2004.

Trikolas, C.J. Geological map of Aigion area 'Aigion sheet'. National Technical University of Athens, Faculty of Mining Engineering and Metallurgy, Section of Geological Sciences, 2005.

Van Houtte, C., Ktenidou, O-J., Larkin, T. and Kaiser, A.: Reference stations for Christchurch, Bulletin of the New Zealand Soc. Earth. Eng., 45(4), 184-195, doi:10.5459/bnzsee.45.4.184-195, 2012.

Wessel, P., Smith, W., Scharroo, R., Luis, J. and Wobbe, F.: Generic mapping tools: improved version released, Eos Trans. AGU, 94(45), 409–410, 2013.

Weatherill, G., Crowley, H., Roullé, A. et al, Modelling site response at regional scale for the 2020 European Seismic Risk Model (ESRM20), Bull Earthquake Eng., 21, 665–714, https://doi.org/10.1007/s10518-022-01526-5, 2023.

Zhu, C., Cotton, F., & Pilz, M.: Detecting Site Resonant Frequency Using HVSR: Fourier versus Response Spectrum and the First versus the Highest Peak Frequency, Bull. Seismol. Soc. Am. 110 (2), 427–440, https://doi.org/10.1785/0120190186, 2020.